



Adsorptive removal of Acidol Red 2BE-NW from aqueous solutions using chitosan/montmorillonite beads

Kamal Benmansour^{a,*}, Soufia Kara Slimane^a, Asma Benosman^b

^aMacromolecules Research Laboratory, Department of Chemistry, Tlemcen University, Imama B.P. 119, Tlemcen, DZ 13000, Algeria, Tel. +213 551833231; emails: kamal.benmansour@mail.univ-tlemcen.dz (K. Benmansour), karamu_48@yahoo.fr (S.K. Slimane)

^bInorganic Chemistry and Environment Laboratory, Department of Chemistry, Tlemcen University, Imama B.P. 119, Tlemcen, DZ 13000, Algeria, email: asma_benosman@yahoo.fr

Received 9 February 2015; Accepted 13 October 2015

ABSTRACT

In this study, the adsorption of the anionic dye Acidol Red 2BE-NW (AR42) on chitosan/montmorillonite (CTS/MMT) is investigated. A series of CTS/MMT beads were prepared by varying the chitosan to montmorillonite ratio and characterized by means of Fourier transform infrared spectroscopy, thermogravimetric analysis, scanning electron microscopy, and X-ray diffraction (XRD) techniques. Batch experiments were carried out to assess the adsorption of AR42 from its aqueous solution using CTS/MMT as the adsorbent surface. Factors influencing control of the adsorption capacity of CTS/MMT such as initial pH value (pH_0), adsorption time, initial dye concentration, chitosan contents, and temperature were investigated. The adsorption curves showed that the adsorption kinetics and isotherms were in good agreement with a pseudo-second-order and Langmuir patterns, respectively, with an observed maximum dye adsorption of 905 mg/g on CTS/MMT (CTS wt% = 25%). These results demonstrated the potential and the outstanding ability of CTS/MMT material for use in the anionic dye adsorption.

Keywords: Chitosan; Montmorillonite; Dye adsorption; Beads

1. Introduction

Water pollution through the discharge of industrial dye effluents is an issue of worldwide environmental concern. Currently, more than 10,000 different synthetic chemical dyes and pigments are known [1]. Colored organic effluents are produced in almost all industries, and by far more extensively in the textile sector [2], which consumes significant amounts of water in the process of dyeing fibers and fabrics,

hence making wastewater highly colored. The concomitantly reduced water transparency severely affects photosynthetic processes by reducing sun ray penetration [3]. Indeed, although many organic compounds are actually biodegradable, the chemical stability and the non-degradability of the structurally complex dyes unravel some of their major drawbacks [4]. More specifically, the xenobiotic nature of the azo-containing dyes has been related to their potential toxicity to aquatic organisms [5]. Thus, the urgent need for practical and economically viable dye removal techniques has become an important as well

*Corresponding author.

as a challenging area which has fostered a large number of research programs directed to wastewater treatment policies.

So far, several dye removal techniques have been developed, including coagulation and flocculation [6], membrane separation [7], oxidation or ozonation [8,9], electro-coagulation [10], and adsorption [11,12]. The latter has proved to be an effective and economical method for dye removal.

Many different types of adsorbents have been reported to be effective in removing color from aqueous effluents. More recently, polysaccharide and clay-based adsorbents have attracted a particular attention. Owing to their biodegradable and non-toxic nature [13], polysaccharide materials are gaining interest for application as adsorbents in wastewater treatment.

Chitosan, a naturally occurring biodegradable and non-toxic polysaccharide derived from chitin deacetylation, has an extremely high affinity for many dye classes [14]. CTS has been shown to be more selective than both conventional ion exchange resins and commercially available activated charcoal and is able to reduce dye concentration to ppb levels. Interestingly, the beads form of CTS shows better adsorption ability than the flake form, due to its higher specific surface area [15]. In contrast, their weak mechanical property (highly swollen in water) and low specific gravity make them rather inconvenient for use as adsorbents in either batch or column modes. Thus, physical and/or chemical modifications of the CTS beads are often undertaken to improve their adsorption performances and to prevent them from dissolution in both strongly acidic or alkali solutions [16,17]. However, such modification procedures seem to be complicated and rather expensive.

On the other hand, natural clay minerals are low-cost materials due to their natural abundance. They display a layered structure which acts as host materials with high sorption properties. Even though natural clays have high adsorption potential, their structural modification has dramatically improved their adsorptive properties [18,19]. In the plethora of clay minerals, montmorillonite has been a material of choice for the removal of organic pigments and dyes [20–23], due to its low cost, large surface area, and high yield cationic exchange.

In this study, we focused our attention on CTS/MMT composite material. The beads form was selected to improve the CTS adsorption ability. AR42, an acidic dye, was chosen for adsorption experiments. Preparation of the composite material and adsorption of AR42 onto CTS/MMT are described. The pH value of the dye solution and the temperature effects on the

adsorption capacity of AR42 on the CTS/MMT beads have been investigated. The adsorption kinetics and isotherms for AR42 adsorption onto CTS/MMT are presented.

2. Experimental

2.1. Chemicals and materials

Samples of medium molecular weight chitosan powder with 85% degree of deacetylation and MMT were supplied by Sigma-Aldrich. Acidol Red® 2BE-NW, a trademark of [2-naphthalenesulfonic acid, 6-amino-4-hydroxy-5-((2-(phenylsulfonyl)phenyl)azo)-, monosodium salt: C₂₂H₁₆N₃NaO₆S₂] (or CI Red 42 or AR42) (Fig. 1) was obtained from BASF. The main properties of this dye are given in Table 1. All chemicals used were of analytical grade and used without further purification. Distilled water was used throughout the adsorption experiments.

2.2. Preparation of CTS/MMT beads. General procedure

A mixture of 2 g chitosan powder and 3 g MMT was suspended in 80 mL (5% v/v) acetic acid and left overnight with stirring. The mixture was then dropped into 500 mL (0.50 M) NaOH solution under continuous stirring at 100 rpm. The resulting beads were then stirred at 200 rpm, and rinsed thoroughly with hot distilled water followed by cold distilled water for several times. The beads were then air-dried before being finally ground and sieved to obtain adsorbent size of <100 μm. This adsorbent size was used throughout the adsorption experiments.

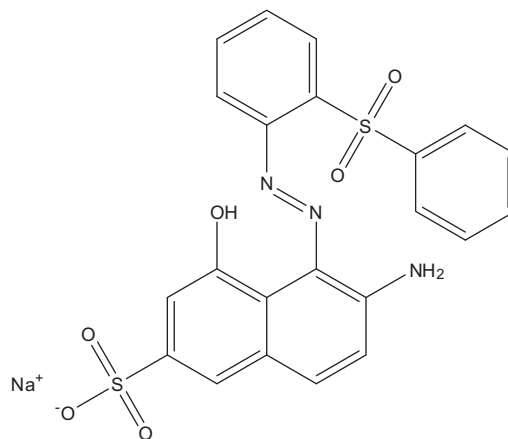


Fig. 1. Chemical structure of AR42.

Table 1
Characteristics of Acidol Red 2BE-NW

Property	Acidol Red 2BE-NW
CI reactive	17,070
Supplier	BASF
Class	Monoazo
Type	Alkali controllable low substantivity
Size (nm)	(1.27 0.88 0.58)
Solubility	>50 g/l
λ_{\max} (nm)	512
M _w (g/mol)	505.5
pK _a	3.6 and 7.1

2.3. Instrumental analysis

2.3.1. FTIR spectroscopy

FTIR spectra of pure chitosan, MMT, and CTS/MMT beads were obtained by Agilent Cary 640 Fourier transform infrared spectroscopy (FTIR) spectrophotometer. Resolution for each spectrum was 2 cm⁻¹.

2.3.2. Thermogravimetric analysis

Thermogravimetric analysis (TGA) was performed under nitrogen flow in the range of 50–800°C on an ATG Q600 TA instruments, at a heating rate of 10°C/min.

2.3.3. SEM measurements

The surface morphology of both CTS and CTS/MMT beads was examined by means of scanning electron microscopy (SEM, Hitachi S4500) at an accelerating voltage of 30 kV attached an X-ray energy dispersive spectrometer, EDS.

2.3.4. XRD analysis

The X-ray diffraction patterns were obtained by a wide-angle X-ray diffractometer (Rigaku D/MAX-RC, Japan) with Cu K α radiation at ambient temperature. The scan rate was 2°/min, and the angle (2 θ) was 5–25°.

2.3.5. pH_{PZC} determination

The point of zero charge pH (pH_{PZC}) of CTS/MMT was determined by the solid addition method [24]. To a series of 100-mL conical flasks, 50 mL of

NaNO₃ solution (0.01 M) of known strength was transferred. The pH₀ values of the solutions were roughly adjusted from 1 to 8 by adding either HNO₃ or NaOH (0.1 mol/L) each. The total volume of the solution in each flask was made exactly to 50 mL by adding the NaNO₃ solution of the same strength. pH of the solutions was then accurately measured, and 1 g of CTS/MMT was added to each flask, which was securely capped immediately. The suspensions were then manually shaken and allowed to equilibrate for 24 h with intermittent manual shaking. The pH values of the supernatant liquid were measured again. The difference between initial (pH₀) and final pH (pH_f) values (pH₀–pH_f) was plotted against pH₀. The point of intersection of the resulting curve with pH₀ axis corresponds to pH_{PZC}. This procedure was repeated for different concentrations of NaNO₃.

2.4. Adsorption experiments

A stock solution of AR42 (250 mg/L) was freshly prepared each time the adsorption experiment was conducted. The stock solution was then diluted to different concentrations. Adsorption experiments were conducted by adding CTS/MMT beads (0.01 g) to AR42 solutions (50 mL) in 100 mL beakers. After adsorption, the solutions were filtered and analyzed under visible light at a wavelength of 510 nm. The initial pH effect on the adsorption of AR42 was studied over a pH domain ranging from 1 to 8. The solution pH was adjusted by adding few drops of 0.10 M HCl or 0.10 M NaOH solutions. The pH study was performed at 400 rpm for 24 h. Time-dependent adsorption of AR42 was conducted with three different concentrations (100, 150, and 200 mg/L) at constant pH 4. A total of 0.01 g of CTS/MMT beads was added to 50 mL of AR42 solutions and stirred for 180 min. The maximum adsorption capacity was determined from the isotherm study.

The amount of AR42 adsorbed, q_e (mg/g), was calculated using the following mass balance Eq. (1):

$$q_e = (C_0 - C_e) \frac{V}{m} \quad (1)$$

where C_0 and C_e are the concentrations of AR42 before and after adsorption (mg/L), V is the volume of the adsorbate used (L), and m is weight of adsorbent used (g).

3. Results and discussion

3.1. Characterization of CTS/MMT beads

3.1.1. Determination of pH_{PZC}

To understand the adsorption mechanism, it is necessary to determine the point of zero charge (pH_{PZC}) of the adsorbent. At pH_{PZC} value, adsorbent surface will have net electrical neutrality. At pH lower than pH_{PZC} , the adsorbent surface is positively charged, while at pH higher than the pH_{PZC} value, negatively charged species will dominate at the adsorbent surface [25]. Thus, cations adsorption is favored at $pH > pH_{PZC}$, while the anions adsorption is favored at $pH < pH_{PZC}$. Fig. 2 shows that for all $NaNO_3$ concentrations, the zero value of pH (pH_0) corresponds to 7.5, which is considered as the pH_{PZC} of the CTS/MMT beads.

3.1.2. FTIR analysis

FTIR analysis of CTS/MMT shows a spectrum that combines the characteristic bands of both CTS and MMT. Indeed, the FTIR spectrum of Na^+ -MMT (Fig. 3(a)) shows the vibration bands at $3,630\text{ cm}^{-1}$ for O–H stretching, $3,442\text{ cm}^{-1}$ due to interlayer and intralayer H-bonded O–H stretching, $1,638\text{ cm}^{-1}$ for H–O–H bending, $1,094$ and $1,038\text{ cm}^{-1}$ for Si–O stretching, 916 and 626 cm^{-1} for Al–OH, 843 and 795 cm^{-1} due to (Al, Mg)–OH vibration modes, and 520 and 467 cm^{-1} for Si–O bending. The spectrum of chitosan (Fig. 3(b)) shows bands at $3,421\text{ cm}^{-1}$ due to the overlapping of O–H and N–H stretching (elongation) bands, $2,913\text{ cm}^{-1}$ for aliphatic C–H stretching, $1,650$ and $1,566\text{ cm}^{-1}$ for N–H bending, $1,421$ and $1,378\text{ cm}^{-1}$ for C–H bending, $1,154$ and $1,070\text{ cm}^{-1}$ for C–O stretching. In Fig. 3(c), the spectrum of the CTS/MMT clearly shows the characteristic absorption combination of

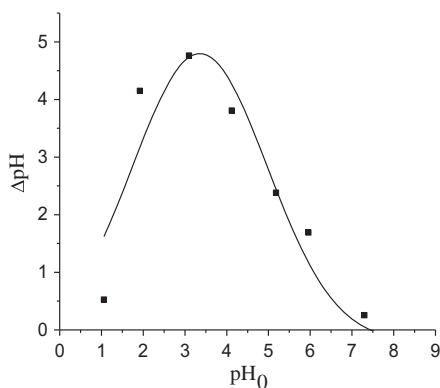


Fig. 2. Determination of pH_{PZC} .

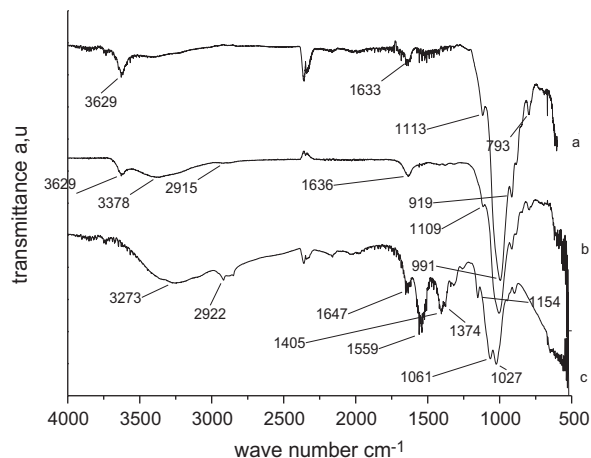


Fig. 3. FTIR spectra of (a) pure chitosan, (b) CTS/MMT bead with 25% of CTS, and (c) MMT.

both chitosan and MMT groups present in the composite material. The band at $1,566\text{ cm}^{-1}$ of the $-NH_2$ group in the starting chitosan was shifted to $1,554\text{ cm}^{-1}$ in the CTS/MMT spectrum, corresponding to the deformation vibration of the protonated amine group ($-NH_3^+$) of chitosan. This $-NH_3^+$ group interacts with the negatively charged sites of MMT. The broad band at $3,430\text{ cm}^{-1}$ can be assigned to stretching vibration of hydroxyl group. The peak at $3,614\text{ cm}^{-1}$ is due to stretching vibration of amine ($-NH_2$) which is consistent with the band at $1,154\text{ cm}^{-1}$ assigned to C–N stretching vibration.

The band at $2,920\text{ cm}^{-1}$ is assigned to C–H stretching vibration of $-CH_2$ and $-CH_3$ groups. The band observed at $1,646\text{ cm}^{-1}$ corresponds to N–H bending vibrations.

3.1.3. Thermogravimetric analysis

The thermal stability of chitosan and CTS/MMT beads was investigated, separately, by TGA under nitrogen flow. Fig. 4 shows the TGA curves of MMT clay, chitosan, and CTS/MMT beads. It was found that the CTS/MMT beads exhibited a higher thermal decomposition in comparison with pure chitosan. Inorganic species have fairly high thermal stabilities, and it is generally believed that their insertion into organic materials increases these latter decomposition temperatures. This can be attributed to the high thermal stability of clay and to the interaction between the clay particles and chitosan [26,27]. The weight loss occurring between ambient temperature and 280°C corresponds to the release of adsorbed water molecules. While it was estimated to ca. $\sim 4\%$ for MMT clay (Fig. 4(a)), chitosan and CTS/MMT beads exhibited a

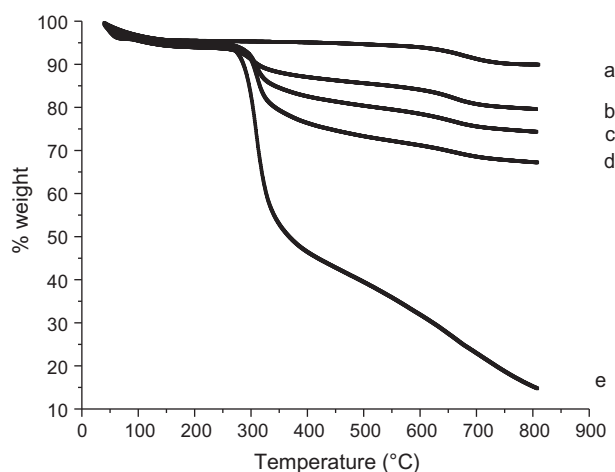


Fig. 4. TGA of CTS/MMT beads with content of CTS in bead: (a) MMT, (b) 15%, (c) 25%, (d) 40%, and (e) chitosan.

slightly higher water loss ranging from 6 to 8% (Fig. 4(b) and (c), respectively). It clearly indicates that the chitosan and CTS/MMT beads have high water retention capacity.

The second stage of decomposition occurred between 300 and 600°C and corresponds to a weight loss of 10–30% for CTS/MMT beads. This is presumably due to the deacetylation and partial degradation of chitosan [28,29]. Remarkably, at 30% weight loss, the exhibited temperature of decomposition of CTS/MMT was 350–400°C higher than that of chitosan. We can safely conclude that CTS/MMT beads are thermally more stable than chitosan membrane. This may be due to a synergistic effect of clay platelets and chitosan in terms of thermal properties.

3.1.4. SEM analysis

Figs. 5a–5c show SEM images of CTS/MMT beads for different wt% at 4,800× magnifications. CTS/MMT structure displays a “flake” particle shape that resembles a corn flake. The presence of chitosan provides lamellar structures. The final morphology of the material depends on the chitosan amount, so that when the chitosan content increases, the lamellar structures display a larger size with better resolution. The sample containing 25% of CTS shows a more opened structure at both the internal and external clay surfaces, while at 40% CTS, accumulation of chitosan at the external clay surfaces tends to make large lamellae closely resembling to the morphology of pure chitosan. As shown in Figs. 5a and 5b, pores smaller than 1 μm are observed on the surface of the CTS/MMT beads. The internal surface area and the presence of pores provide suitable sites for AR42 adsorption.

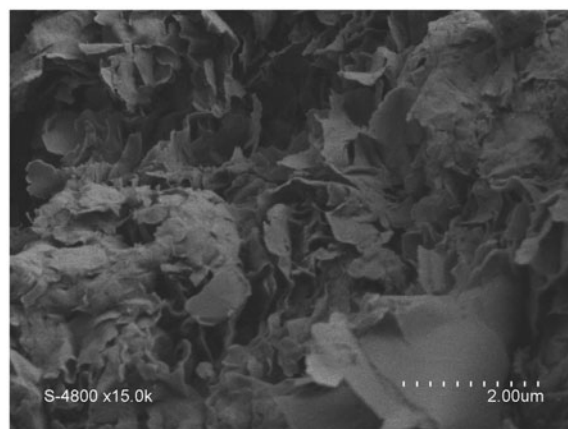


Fig. 5a. SEM morphology of CTS/MMT beads with amount CTS of 15%, increasing 2 μm.

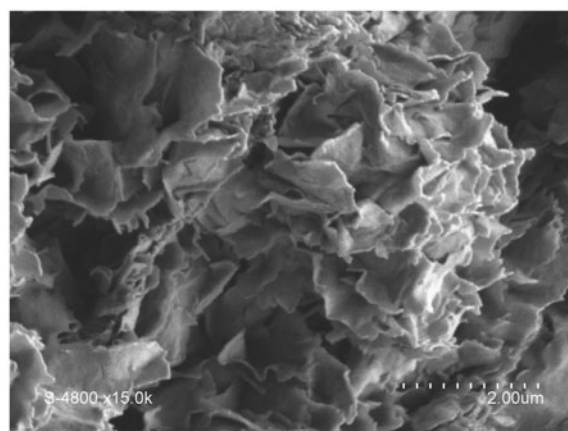


Fig. 5b. SEM morphology 25% CTS in beads, increasing 2 μm.

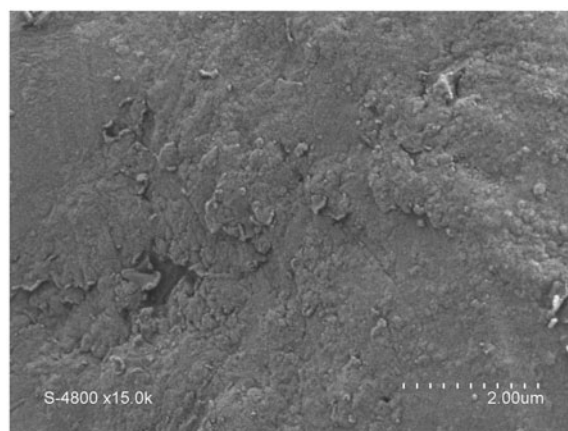


Fig. 5c. SEM morphology 40% CTS in beads, increasing 2 μm.

3.1.5. X-ray diffraction analysis

X-ray diffraction (XRD) is a powerful technique for the investigation of the intercalation pattern of montmorillonite. The XRD patterns of MMT and CTS/MMT containing two beads with different chitosan contents wt% = 25 and 40% are shown in Fig. 6(a)–(c), respectively. The XRD pattern of MMT (Fig. 6(a)) shows a typical diffraction peak at 6.94° , corresponding to a basal spacing of 1.274 nm. Upon intercalation with CTS, this peak shifts to lower angle. A diffraction peak is observed at 5.78° ($d = 1.53$ nm) for CTS/MMT samples which means that the intercalation has occurred and the intercalated beads have been formed (Figs. 6(b) and (c)).

3.2. pH effect on dye adsorption

The relationship between dye solution pH and its adsorption process is of paramount importance, particularly in terms of adsorption capacity. pH variations of the solution are primarily related to the following: (1) the surface charge of the adsorbent, (2) the ionization degree of the adsorptive dye, and (3) the extent of ionic dissociation of the functional groups that are present in the active sites of the adsorbent.

In order to assess the pH effect on the magnitude of adsorption, dye solution pH was varied from 1 to 9.

Fig. 7 illustrates the adsorption pattern (curves) relative to pH variation. Dye adsorption remained constant at (ca. 750 mg/g) in pH zone ranging from 1 to 3, and then decreased from 750 to 200 mg/g while increasing pH from 4 to 9. Consequently, pH 4 was selected for subsequent adsorption experiments. This result is in good agreement with our previous expectations. Indeed, at pH 4 which is lower than pH_{PZC} (7.5), the surface of the adsorbent is positively charged. The anionic ($R-SO_3^-$) groups present in dye molecules are attracted to the protonated amine groups of chitosan. Adsorption capacity reached its maximum when all of dye anionic groups are electrostatically bonded to CTS surface. In contrast, in alkaline solution, deprotonation of amine group takes place and eventually results in poor interaction between dye and adsorbent. Moreover, the excessive hydroxyl ions present in solution may compete with the dye anions and a slow decrease in dye uptake was observed.

3.3. Effect of chitosan content on adsorption

The performance of CTS/MMT beads for AR42 adsorption as a function of CTS contents (wt%) was further investigated. So far, it appears that CTS ratio is a determining factor in the adsorption process. As illustrated in Fig. 8, when 25% (by weight) of CTS were

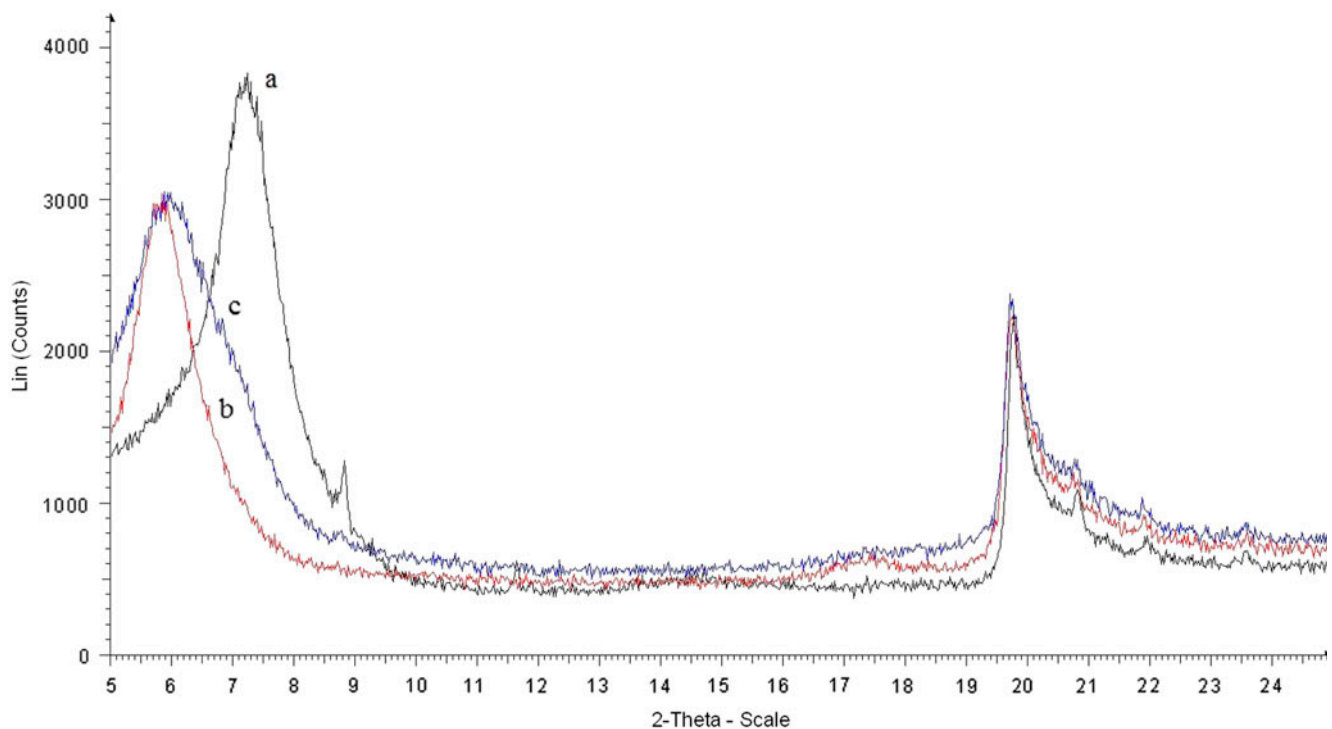


Fig. 6. XRD patterns of MMT (a) beads with chitosan content wt% = 25% (b), and 40% (c).

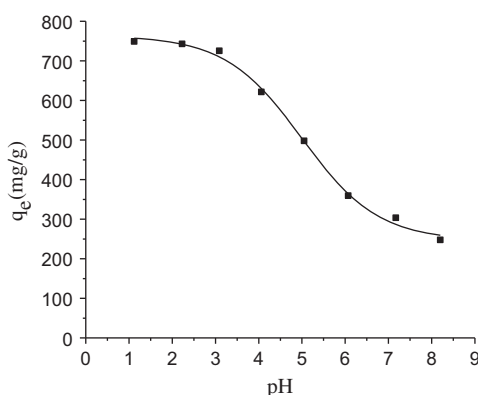


Fig. 7. pH effect on the adsorption capacity of CTS/MMT (25%) bead for AR ($C_0 = 150$ mg/L).

introduced, the adsorption increased from 100 up to 720 mg/g, and then decreased to 645 mg/g when CTS contents were adjusted to 40%. This increase in adsorption seems to be the result of two processes acting synergistically: on the one hand, a pores enlargement due to CTS intercalation thus favoring dye penetration, and on the other hand, an electrostatic interaction between chitosan and the anionic dye. However, the adsorption capacity of the beads is reversed when it reaches a limit of ca. ~25 wt% of CTS beyond which it starts decreasing. This might be attributed to a more intensive interaction between MMT and CTS—while increasing CTS contents—, thus lowering the number of available adsorption sites. Therefore, a fixed ratio of CTS/MMT beads with 25% CTS contents was selected for the remaining discussion.

3.4. Effect of temperature

The temperature effect on the sorption process was performed over the range of 300–320 K. It was

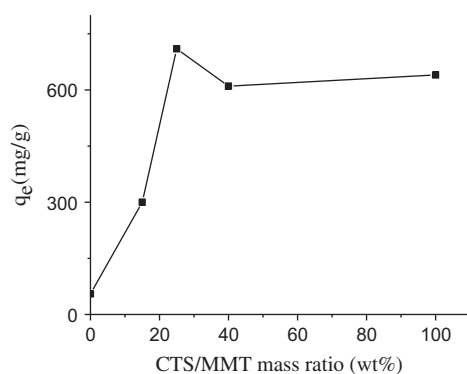


Fig. 8. Effect of the chitosan content on the adsorption capacity for AR ($C_0 = 150$ mg/L).

observed that by increasing the temperature, sorption of AR42 decreases (Fig. 9). This might be partly attributed to a chitosan desorption from MMT surface. Indeed, by increasing temperature there is an inherent global energy increase of the intercalated polyelectrolyte which possibly allows some of their moieties to leave MMT active centers. As a result, the amount of adsorbed dye decreases.

3.5. Equilibrium studies

3.5.1. Effect of initial dye concentration

Three concentrations of dye (100, 150, and 200 mg/L) were used for this study and the adsorption data are (summarized, presented, described) in Fig. 10. The results showed a fast dye binding to the sorbent during the first few minutes, followed by a slow increase until a state of equilibrium was reached. The initial rapid phase may likely be due to the large number of vacant sites available initially. It follows an increase in adsorbate concentration gradient between the solution and the adsorbent [30]. It is generally admitted that when a surface reaction process is involved, the initial adsorption step is fast. Then, a slower rate would follow as the available adsorption sites gradually decrease. Fig. 10 also shows that the adsorption capacity of the beads rises sharply from 450 to 905 mg/g when C_0 of dye was increased from 100 to 200 mg/L. A rapid adsorption of AR42 occurred in the first 20 min for 100 mg/L, and within 30 min for both 150 and 200 mg/L solutions. We understand that the adsorption process is intimately related to the difference in dye concentration in solution and at the adsorbent surface. Hence, its initial concentration provides the driving force which overcomes the resistance to dye transfer from aqueous phase to the adsorbent surface. Additionally, a higher dye initial concentration should enhance dye–adsorbent interaction, and thus, we

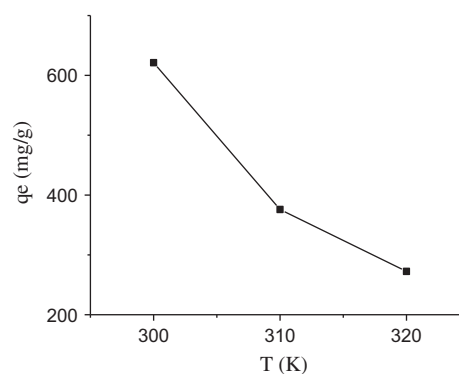


Fig. 9. Effect of temperature on adsorption capacity of CTS/MMT (25%) bead for AR ($C_0 = 150$ mg/L).

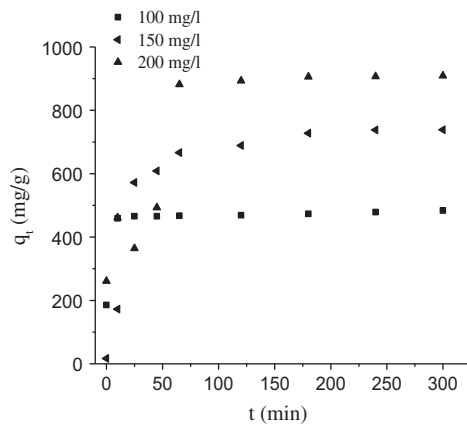


Fig. 10. Effect of initial concentration of AR42 on adsorption capacity of CTS/MMT (25%) bead.

expect a stronger driving force which results ultimately in a higher adsorption.

3.5.2. Adsorption equilibrium models

Adsorption data were fit to the Langmuir and Freundlich isotherms. The Langmuir isotherm is valid for monolayer sorption owing to the finite surface number of identical sites and expressed in the linear form as in Eq. (2):

$$\frac{C_e}{q_e} = \frac{1}{bq_{\max}} + \frac{C_e}{q_{\max}} \quad (2)$$

where C_e is the equilibrium concentration (mg/L) and q_e is the amount adsorbed at equilibrium (mg/g). The Langmuir constant q_{\max} (mg/g) represents the monolayer adsorption capacity, and b (L/mg) is related to the heat of adsorption. The Langmuir isotherm adsorption equation can also be expressed by means of R_L , a dimensionless constant referred to as separation factor or equilibrium parameter, predicting whether an adsorption system is favorable or unfavorable. R_L is calculated using the following Eq. (3):

$$R_L = \frac{1}{1 + bC_0} \quad (3)$$

where C_0 is the initial dye concentration (mg/L). If R_L values lie between 0 and 1, the adsorption is favorable.

The Freundlich isotherm describes the heterogeneous surface energies by multilayer adsorption and is expressed in a linear form as in Eq. (4):

$$\ln q_e = \ln K_F + \frac{1}{n} \ln C_e \quad (4)$$

where K_F is the adsorption capacity (mg/g), and n , an empirical parameter related to the intensity of adsorption, which varies with the adsorbent heterogeneity. The greater the value of n , the more favorable the adsorption is.

The obtained equilibrium data fit more to Langmuir model (Fig. 11) than to Freundlich model (Fig. 12), indicating a monolayer adsorption pattern. From Langmuir isotherm curves, q_{\max} was easily calculated to be 409.83 mg/g. This result indicates that the adsorbent has a high capacity to remove AR42 dye from the solution.

The values of Langmuir and Freundlich constants are presented in Table 2. The shape of the isotherm curve is determined by the R_L parameter, accordingly:

$R_L > 1$, unfavorable adsorption.

$0 < R_L < 1$, favorable adsorption.

$R_L = 0$, irreversible adsorption.

$R_L = 1$, linear adsorption.

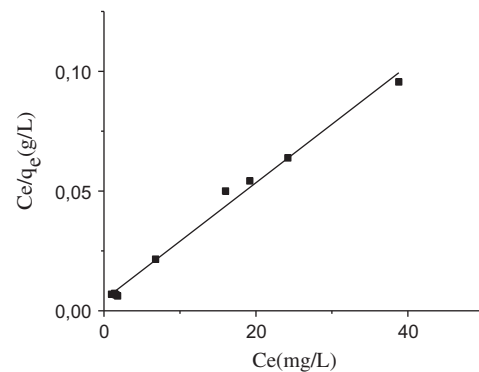


Fig. 11. Langmuir plot for the adsorption of AR42 by CTS/MMT (25%) beads.

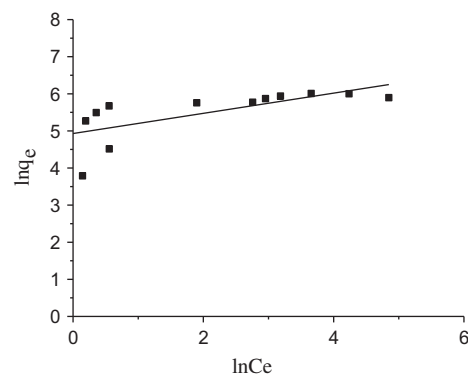


Fig. 12. Freundlich plot for the adsorption of AR42 by CTS/MMT (25%) beads.

The calculated R_L value was 0.0124 ($C_0 = 150$ mg/L) indicating that the adsorption of AR42 on beads is favorable at studied temperature.

The Gibbs free energy change (ΔG) for adsorption at 300 K was calculated using Eq. (5):

$$\Delta G = -RT \ln b \tag{5}$$

where R is the gas constant (8,314 J/mol K), T (K) is the absolute temperature, and b (L/mg) is the Langmuir constant. The calculated ΔG value is -3.82 kJ/mol, which is consistent with the spontaneous nature of the adsorption and confirms the affinity of AR42 for CTS/MMT surface. As a matter of fact, the chemical structure of the dye, the adsorbent nature, and its physicochemical properties are determinant factors in the adsorption pattern. In this study, the adsorption occurs preferentially by ionic interaction between the dye sulfonate group and the chitosan amino group.

3.6. Adsorption kinetic studies

Fig. 13 shows the contact time vs. AR42 adsorption on CTS, MMT, and CTS/MMT beads with different chitosan content, respectively. It appears that the adsorption on CTS, MMT, and the beads increased rapidly at the beginning and then gradually with longer adsorption time until equilibrium was reached. The adsorption equilibrium of AR42 on beads was reached after 750 min.

The efficiency and the dynamics of the adsorption are best described by kinetic studies. It allows the prediction (assessment) of adsorption rate and provides valuable insight for further modeling and designing full-batch experiments. In order to gain a better understanding of the adsorption mechanism and some of its important aspects, such as mass transfer and complex reaction pathway, the experimental data were conjectured with theoretical pseudo-first-order and pseudo-second-order adsorption as well as an intra-particle diffusion model.

A simple pseudo-first-order kinetic model, suggested by Lagergren [31], can be used to describe

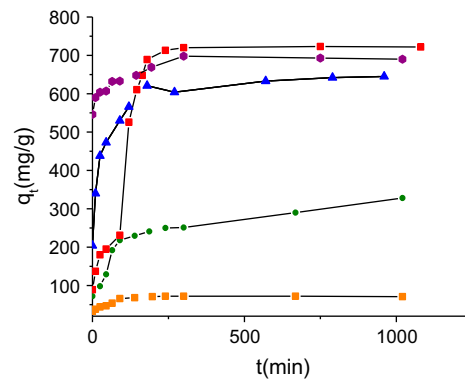


Fig. 13. Effect of the contact time on adsorption capacity of CTS/MMT bead for AR42 ($C_0 = 150$ mg/L).

the adsorption of solid/liquid systems. It assumes that the rate of solute uptake is directly proportional to the decrease in dye concentration between a saturated solution and the adsorbed amount and may be expressed as in Eq. (6):

$$\log(q_e - q_t) = \log q_e - \frac{k_1 t}{2.303} \tag{6}$$

where k_1 is the pseudo-first-order rate constant (min^{-1}), q_e and q_t are the amounts of adsorbed dye (mg/g) at equilibrium and at time t (min).

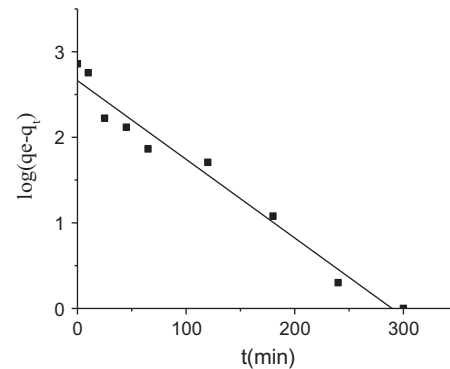


Fig. 14a. Pseudo first order model for the adsorption of AR by CTS/MMT nanocomposite ($C_0 = 150$ mg/L).

Table 2
Adsorption isotherms constants for the adsorption of AR42 on CTS/MMT beads (25%)

Sample	Langmuir			Freundlich		
	R^2	b (L/mg)	q_{\max} (mg/g)	R^2	K_F (mg/g)	n
CTS/MMT	0.990	0.53	409.83	0.492	182.47	2.944

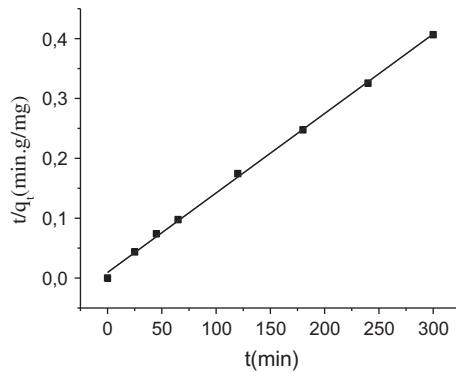


Fig. 14b. Pseudo second order model for the adsorption of AR by CTS/MMT nanocomposite ($C_0 = 150$ mg/L).

The plot of $\log(q_e - q_t)$ vs. t gives a straight line with a slope of $k_1/2.303$ and intercept $\log q_e$, (Fig. 14a).

A pseudo-second-order kinetic model, involving a rate-determining step corresponding to the chemical adsorption has been proposed [32], and stated by Eq. (7):

$$\frac{t}{q_t} = \frac{1}{k_2 q_e^2} + \frac{t}{q_e} \quad (7)$$

where k_2 (g/mg/min) is the rate constant of the pseudo-second-order adsorption. The plot of t/q_t vs. t gives a straight line with a slope of $1/q_e$ and intercept $1/k_2 q_e^2$ (Fig. 14b).

Another tool of significant importance in terms of kinetics evaluation is the Weber and Morris intraparticle diffusion model [33] which highlights the relationship between specific sorption and $t^{1/2}$, according to Eq. (8):

$$q_t = k_i t^{1/2} + C \quad (8)$$

where q_t is the fraction dye uptake (mg/g) at time t , k_i is the intra-particle diffusion rate constant (mg/g min^{1/2}), and C is the intercept (mg/g).

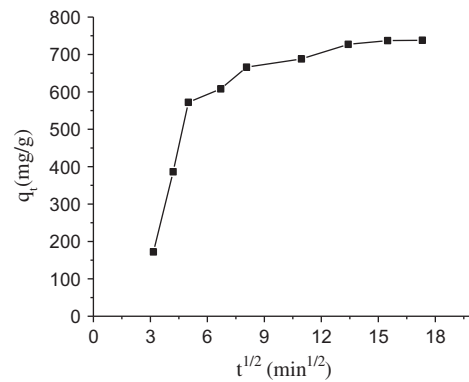


Fig. 14c. Intraparticle diffusion model of CTS/MMT nanocomposite ($C_0 = 150$ mg/L).

The results of the kinetic parameters for AR42 adsorption are summarized in Table 3. The experimental $q_{e,exp}$ and calculated $q_{e,cal}$ values for pseudo-second-order model are very close. In addition, the calculated correlation coefficients are almost constant. These results are consistent with a pseudo-second-order adsorption of AR42 on CTS/MMT beads.

The intra-particle-diffusion plot gave multi-linearity, signifying the different stages represented by q_t vs. $t^{0.5}$ plot. Fig. 14c shows three linear sections: Dye molecules move to the external surface of the beads through film diffusion, indicating a boundary layer effect. Then, dye molecules penetrate into the beads, through the pores, by intra-particle diffusion mechanism. The third step refers to equilibrium state. It is worth mentioning that any of the straight portions of the curve pass through the origin. It should be stressed out that even if intra-particle diffusion is involved in the adsorption process, it is not the only rate-determining step. Comparison of k_i values (Table 3) reveals that the initial diffusion step is very fast, and the rate is proportional to dye concentration. The second step is much slower. As the departure from the intraparticle mechanism indicates some influence of boundary layer diffusion control, it is likely that the dye concentration impairs the

Table 3
Kinetic parameters of CTS/MMT (25%) beads at different concentration of AR42

C_0 (mg/L)	Pseudo-first-order					Pseudo-second-order		Intraparticle diffusion			
	$q_{e,exp}$ (mg/g)	R_1^2	$q_{e,cal}$ (mg/g)	k_1 (min ⁻¹)	R_2^2	$q_{e,cal}$ (mg/g)	k_2 (g/mg min)	k_{i1} (mg/g min ^{0.5})	k_{i2}	k_{i3}	R_3^2
100	483	0.662	53.70	0.0118	0.991	486.8					
150	737	0.967	459.19	0.0211	0.998	751.87	0.000018	217.62	30.28	8.531	0.933
200	905	0.866	457.08	0.0206	0.999	925.92	0.000025				

molecules' ability to approach the surface, thus influencing the rate of adsorption.

4. Conclusion

In this study, results of adsorption using chitosan/montmorillonite beads for the removal of AR42 from aqueous solutions were presented. This adsorbent exhibited interesting sorption properties toward anionic dye (the maximum adsorption capacity was 905 mg/g), depending on the presence of sulfonate groups. The adsorption process, however, was affected by several physicochemical factors such as pH, chitosan content, dye concentration, and temperature. The equilibrium experimental data fit perfectly with the Langmuir isotherm. It implies the monolayer formation of the surface on the beads by dye molecules. Kinetic data of adsorption were well fitted by the pseudo-second-order kinetic model. The sorption mechanism was a multi-step process, involving adsorption on the external surface, diffusion into the bulk and electrostatic interactions.

Acknowledgments

The authors are thankful to Professor André Deratani, Research Director at the European Institute of Membranes (Montpellier, France), for SEM analysis. Professor Ulrich Maschke, at UMET University of Lille, France, is also gratefully acknowledged for his helpful assistance in TGA measurements.

References

- [1] L. Donnaperna, L. Duclaux, R. Gadiou, M.P. Hirn, C. Merli, L. Pietrelli, Comparison of adsorption of Remazol Black B and Acidol Red on microporous activated carbon felt, *J. Colloid Interface Sci.* 339 (2009) 275–284.
- [2] M.S. Chiou, P. Ho, H.-Y. Li, H.Y. Li, Adsorption of anionic dyes in acid solutions using chemically cross-linked chitosan beads, *Dyes Pigm.* 60 (2004) 69–84.
- [3] C.M. Kao, M.S. Chou, W.L. Fang, B.W. Liu, B.R. Huang, Regulating colored textile wastewater by 3/31 wavelength admittance methods in Taiwan, *Chemosphere* 44 (2001) 1055–1063.
- [4] G. Crini, Non-conventional low-cost adsorbents for dye removal: A review, *Bioresour. Technol.* 97 (2005) 1061–1085.
- [5] M.N.V.R. Kumar, T.R. Sridhari, K.D. Bhavani, P.K. Dutta, Trends in color removal from textile mill effluents, *Colorage* 40 (1998) 25–34.
- [6] J. Panswed, S. Wongchaisuwan, Mechanism of dye wastewater color removal by magnesium carbonate-hydrated basic, *Water Sci. Technol.* 18 (1986) 139–144.
- [7] G. Ciardelli, L. Corsi, M. Marucci, Membrane separation for wastewater reuse in the textile industry, *Resour. Conserv. Recycl.* 31 (2000) 189–197.
- [8] K. Swaminathan, S. Sandhya, A. Carmalin Sophia, K. Pachhade, Y.V. Subrahmanyam, Decolorization & degradation of H-acid and other dyes using ferrous hydrogen peroxide system, *Chemosphere* 50 (2003) 619–625.
- [9] M. Muthukumar, N. Selvakumar, Studies on the effect of inorganic salts on decolouration of acid dye effluents by ozonation, *Dyes Pigm.* 62 (2004) 221–228.
- [10] A. Alinsafi, M. Khemis, M.N. Pons, J.P. Leclerc, A. Yaacoubi, A. Benhammou, A. Nejmeddine, Electro-coagulation of reactive textile dyes and textile wastewater, *Chem. Eng. Process.* 44 (2005) 461–470.
- [11] I.D. Mall, V.C. Srivastava, N.K. Agarwal, I.M. Mishra, Removal of congo red from aqueous solution by bagasse fly ash and activated carbon: Kinetic study and equilibrium isotherm analyses, *Chemosphere* 61 (2005) 492–501.
- [12] I.D. Mall, V.C. Srivastava, G.V.A. Kumar, I.M. Mishra, Characterization and utilization of mesoporous fertilizer plant waste carbon for adsorptive removal of dyes from aqueous solution, *Colloids Surf., A* 278 (2006) 175–187.
- [13] M. Auta, B.H. Hameed, Chitosan–clay composite as highly effective and low-cost adsorbent for batch and fixed-bed adsorption of methylene blue, *Chem. Eng. J.* 237 (2014) 352–361.
- [14] R. Dolphen, N. Sakkayawong, P. Thiravetyan, W. Nakbanpote, Adsorption of Reactive Red 141 from wastewater onto modified chitin, *J. Hazard. Mater.* 145 (2007) 250–255.
- [15] F.C. Wu, R.L. Tseng, R.S. Juang, Comparative adsorption of metal and dye on flake- and bead-types of chitosans prepared from fishery wastes, *J. Hazard. Mater.* 73 (2000) 63–75.
- [16] E. Guibal, M. Jansson-Charrier, I. Saucedo, P. Cloirec, Enhancement of metal ion sorption performances of chitosan: Effect of the structure on the diffusion properties, *Langmuir* 11 (1995) 591–598.
- [17] A.R. Nešić, S.J. Veličković, D.G. Antonović, Modification of chitosan by zeolite A and adsorption of Bezactive Orange 16 from aqueous solution, *Composites Part B* 53 (2013) 145–151.
- [18] O. Ozdemir, B. Armagan, M. Turan, M.S. Çelik, Comparison of the adsorption characteristics of azo-reactive dyes on mesoporous minerals, *Dyes Pigm.* 62 (2004) 49–60.
- [19] Y. Peng, D. Chen, J. Ji, Y. Kong, H. Wan, C. Yao, Chitosan-modified palygorskite: Preparation, characterization and reactive dye removal, *Appl. Clay Sci.* 74 (2013) 81–86.
- [20] A.R. Nesic, S.J. Velickovic, D.G. Antonovic, Characterization of chitosan/montmorillonite membranes as adsorbents for Bezactive Orange V-3R dye, *J. Hazard. Mater.* 209–210 (2012) 256–263.
- [21] S. Kittinaovarat, P. Kansomwan, N. Jiratumnukul, Chitosan/modified montmorillonite beads and adsorption of Reactive Red 120, *Appl. Clay Sci.* 48 (2010) 87–91.
- [22] P. Lertsutthiwong, K. Noomun, S. Khunthon, S. Limpanart, Influence of chitosan characteristics on the properties of biopolymeric chitosan/montmorillonite, *Prog. Nat. Sci.* 22 (2012) 502–508.
- [23] L. Wang, A. Wang, Adsorption characteristics of Congo Red onto the chitosan/montmorillonite nanocomposite, *J. Hazard. Mater.* 147 (2007) 979–985.

- [24] L.S. Balistreri, J.W. Murray, The surface chemistry of goethite (α FeOOH) in major ion seawater, *Am. J. Sci.* 281 (1981) 788–806.
- [25] L. Monser, N. Adhoum, Tartrazine modified activated carbon for the removal of Pb(II), Cd(II) and Cr(III), *J. Hazard. Mater.* 161 (2008) 263–269.
- [26] J.H. Chang, Y.U. An, G.S. Sur, Poly(lactic acid) nanocomposites with various organoclays. I. Thermo-mechanical properties, morphology, and gas permeability, *J. Polym. Sci., Part B: Polym. Phys.* 41 (2003) 94–103.
- [27] K.E. Strawhecker, E. Manias, Structure and properties of poly(vinyl alcohol)/Na⁺ montmorillonite nanocomposites, *Chem. Mater.* 12 (2000) 2943–2949.
- [28] F.A.A. Tirkistani, Thermal analysis of some chitosan Schiff bases, *Polym. Degrad. Stab.* 60 (1998) 67–70.
- [29] X. Qu, A. Wirsén, A.C. Albertsson, Effect of lactic/glycolic acid side chains on the thermal degradation kinetics of chitosan derivatives, *Polymer* 41 (2000) 4841–4847.
- [30] G. Crini, Kinetic and equilibrium studies on the removal of cationic dyes from aqueous solution by adsorption onto a cyclodextrin polymer, *Dyes Pigm.* 77 (2008) 415–426.
- [31] S. Lagergren, About the theory of so-called adsorption of soluble substances, *K. Sven. vetensk.akad. handl.* 24 (4) (1898) 1–39.
- [32] Y.S. Ho, G. McKay, Pseudo-second order model for sorption processes, *Process Biochem.* 34(5) (1999) 451–465.
- [33] J.W.J. Weber, J.C. Morriss, Kinetics of adsorption on carbon from solution, *J. Sanit. Eng. Div. Am. Soc. Civil Eng.* 89 (1963) 31–60.